Conf-9206172--5

Thermal, Structural and Diffraction Analyses of a Gallium-cooled X-ray Monochromator*

C.S. Rogers, A.T. Macrander and D.M. Mills
Advanced Photon Source
Argonne National Laboratory
9700 South Cass Avenue
Argonne, IL 60439

ANL/CP--76521

DE92 017063

June, 1992

cz

*This work supported by the U.S. Department of Energy, BES-Materials Sciences, under contract no. W-31-109-ENG-38

Thermal, structural and diffraction analyses of a gallium-cooled x-ray monochromator

C. S. Rogers, A. T. Macrander and D. M. Mills

Argonne National Laboratory, Advanced Photon Source
Argonne, IL 60439

ABSTRACT

The next generation of synchrotron radiation sources will produce very high power and power density x-ray beams. For example, the Advanced Photon Source (APS) under construction at Argonne National Laboratory will produce beams containing up to 5 kW of power and peak normal power densities in excess of 150 W/mm^2. Normally, the first optical component to intercept the x-ray beam is a crystal monochromator. This device typically uses a single crystal of silicon or germanium as a band-pass filter according to Braggs' law of diffraction. Under the severe heat loading of modern synchrotron beams, the performance of the monochromator is degraded by reducing the photon throughput and increasing the beam divergence.

This paper describes the methods used to calculate the thermally induced deformations in standardly configured monochromator crystals using finite element analysis. The results of these analyses are compared to recent experiments conducted at the Cornell High Energy Synchrotron Source (CHESS) using a high-performance, gallium-cooled crystal. Computer simulations can be used to evaluate the performance of high-heat-load x-ray optics for future synchrotron sources.

1. INTRODUCTION

Third generation synchrotrons are under construction in Europe, Japan, and the United States. These machines are distinguished from their predecessors by the fact that they have low-emittance lattices, high storage ring current and energy, and have been optimized to include many insertion devices. The APS will operate with a positron energy of 7 GeV and a stored current of 100 mA.[1] The worst heat load problem occurs for undulators because the natural opening angle of these beams is very small and the total power is confined to a narrow solid angle. For APS-style undulators, the peak normal power density 30 m from the source can be as high as 180 W/mm^2.

The challenge faced by researchers is to develop first optical components that can handle these high heat loads without serious degradation of performance. Currently, there are no x-ray sources available with a large enough total power and power density to test new cooling schemes. Therefore, the capabilities have been developed at Argonne over the past several years to apply the finite element method to calculate the deformation due to thermal stress of crystal optics and then to calculate the impact on diffraction.

Recently, experiments were performed at CHESS using an APS prototype undulator to test the performance of a liquid-gallium-cooled monochromator.[2] This undulator produces a moderately high total power, about 240 W at 60 mA, and a peak normal power density of about 30 W/mm^2 at 18 m from the source.

In this paper, finite element analysis using the ANSYS[3] program is used to model the thermal response and structural deformation of the gallium-cooled monochromator crystal. Rocking curves are then calculated and compared to the experimental data. Once a baseline of confidence in the simulations is established, the analysis may be extended to situations for which there is no experimental data, such as a more intense beam, different crystal geometries and cooling fluids, and different flow rates. It is shown

that this method of analysis can be used to accurately predict the performance of crystal optics under the high heat loads of modern synchrotron sources.

2. THE UNDULATOR

The x-ray source used in these experiments is an APS prototype undulator installed at CHESS. An undulator is a periodic magnetic device used to produce quasi-monochromatic x-rays. The radiation produced by the undulator is emitted in a highly collimated beam. A detailed description of this undulator is given by Bilderback, et al.[4] The insertion device and electron storage ring parameters are given in Table 1.

Table 1. Insertion device and storage ring parameters.

Storage ring energy, E_R(GeV)	5.434	Undulator period, λ (cm)	3.3
Horizontal β function, β_H (m)	19.95	Undulator gap, (mm)	17
Vertical β function, β_V (m)	4.45	Undulator length, L (m)	2.03
Relativistic factor, $1/\gamma$ (mrad)	0.094	Number of poles, N	123
Horizontal source size, σ_H (mm)	1.16	Peak field on-axis, $B0$ (T)	0.35
Vertical source size, σ_V (mm)	0.076	Deflection parameter, K	1.1
Horizontal divergence, σ'_H (μrad)	56	Normalization factor, $G(K)$	0.95
Vertical divergence, σ'_V (μrad)	17	Measured power, (W/mA)	3.95

2.1 Undulator power distribution

One of the most important parameters to consider in the design of synchrotron optics is the spatial distribution of the frequency integrated power. Calculations for the power spectrum have been reported by Kim.[5] The spatial distribution of the frequency integrated power normal to the beam direction is given by,

$$\frac{dP}{dx\,dy} = \left[P_T \frac{21\gamma^2}{16\pi K D^2} G(K) \right] f_K(x,y) \tag{1}$$

where x and y are the horizontal and vertical directions, respectively. The total power integrated over all angles and frequencies is P_T , $\gamma$is the relativistic factor, K is the deflection parameter, $G(K)$ is a normalization factor depending only on K, D is the distance from the source, and f_K is a normalized angular distribution function. At the origin, $f_K(0,0) = 1$ and the term in brackets represents the peak power density. For a deflection parameter near unity, the normalized angular distribution function is approximated by a gaussian function in the vertical and a parabolic function in the horizontal. Therefore, the distribution function can be written in Cartesian coordinates for the origin at the center of the beam as follows,

$$f_K(x,y) \equiv e^{-y^2/2\sigma^2} \left[1 - \left(\frac{x}{x_0} \right)^2 \right] \tag{2}$$

where σ is the gaussian standard deviation, and $2x_0$ is the beam width. At 18 m from the source, the beam footprint at normal incidence was calculated to be approximately 7.8 mm in the horizontal and 4.5 mm vertically. The total power in the x-ray beam is given by,

$$P_T = P_P \int_{-\infty}^{\infty} \left[\int_{-x_0}^{x_0} f_K(x,y)\,dx \right] dy \tag{3}$$

where P_P is the peak power density. Integrating this equation we obtain,

$$P_T = \frac{4\sqrt{2\pi}}{3} \sigma x_0 P_P \tag{4}$$

Eqs. (1) and (4) may be solved for P_P, set equal to each other and solved for the standard deviation of the gaussian resulting in the following,

$$\sigma = \frac{12\pi K D^2}{21\sqrt{2\pi}\,\gamma^2 G(K) x_0} \tag{5}$$

Eq. (1) may be integrated to determine the power in the beam over some interval giving,

$$P(\Delta x, \Delta y) = P_P \left[x_2 - x_1 + \frac{(x_1 - x_2)^3}{3x_0^2} \right] \left[\frac{\sigma\sqrt{2\pi}}{2} \left\{ erf\left(\frac{y_2}{\sigma\sqrt{2}} \right) - erf\left(\frac{y_1}{\sigma\sqrt{2}} \right) \right\} \right] \tag{6}$$

The total power as a function of current was measured during the experiment. Therefore, the peak power can be solved for from Eq. (4), and this value substituted into Eq. (6) to determine the power deposited over any element on the crystal surface. The spatial distribution of power from the undulator for an electron current of 60 mA is shown in Fig. 1.

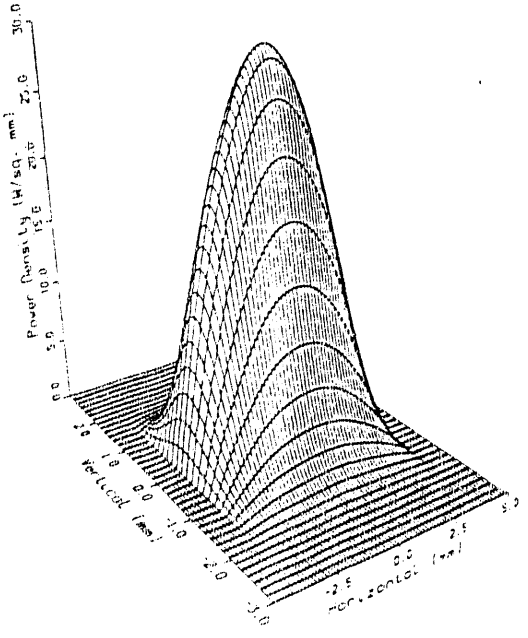

Fig 1. Normal power density for APS/CHESS undulator at 60 mA, 18 m from the source.

3. EXPERIMENTAL SUMMARY

The first crystal was cooled by pumping liquid gallium through 1 mm wide slots cut beneath the diffraction surface. The slots were spaced 0.55 mm apart and were 0.75 mm below the surface. The crystal was oriented in the (111) direction. A schematic of the crystal is shown in Fig. 2. The top plate of the monochromator crystal was bonded to a second piece of silicon. This crystal assembly was secured to a stainless steel fluid distribution manifold using rubber o-rings. The total flow rate for all experimental data was 1 gpm. The gallium was pumped using an electromagnetic induction pump developed at Argonne.[6]

The monochromator was tuned to 5 keV, and rocking curve measurements were made at storage ring currents ranging from 2 to 60 mA. It was determined that the diffracted intensity began to decrease due to thermal deformation between 20 and 30 mA.

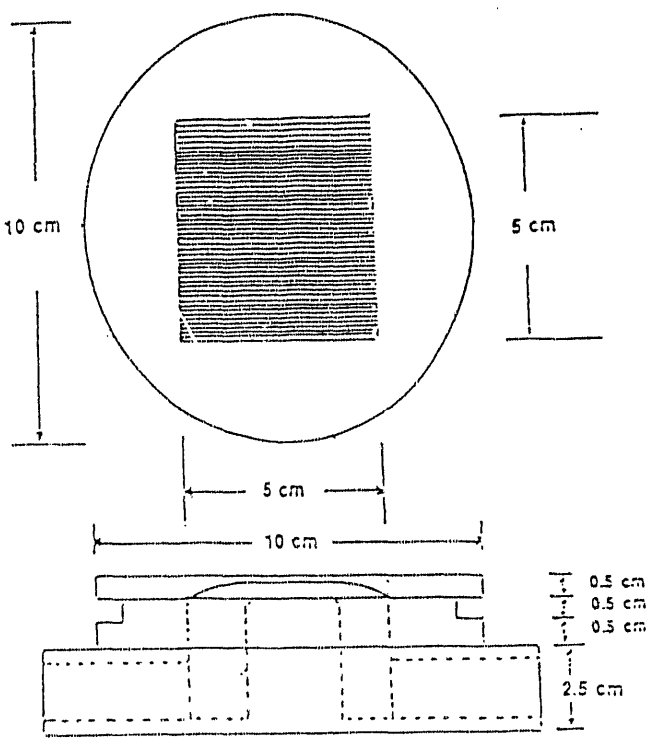

Fig. 2. Schematic of the liquid-gallium-cooled first crystal.

4. THERMAL ANALYSIS

4.1 Power absorption

The first step in the thermal analysis is to determine the heat loading on the face of the crystal. The energy of the x-rays is absorbed over some finite depth into the crystal. The intensity of the x-rays

decreases exponentially with the depth of penetration. For the analysis, it was assumed that the energy is deposited uniformly in a top layer of the crystal. A critical energy can be defined for the undulator by the following equation

$$E_c = 0.6651 E_R^2 B_0 \tag{7}$$

Approximately half of the power contained in the beam is below this energy and half is above. The critical energy for this case is about 7 keV. Therefore, this energy was used to determine the depth of penetration to 10 percent of the incident intensity. The power over each element on the crystal surface was calculated from Eq. (6) and deposited uniformly in the top 0.05 mm of the crystal. An analysis was performed using the Photon[7] program to determine a more accurate absorption profile. It was found that about 70 percent of the power was absorbed in the top 0.05 mm. Therefore, it is believed that the above procedure yields a simple and accurate estimate of the absorption profile. The x-ray beam is intercepted by the first crystal at the Bragg angle, θ, and the footprint of the beam is spread out in the vertical direction by a factor of $(sin\theta)^{-1}$.

4.2 Thermal finite element analysis

The power from the x-ray beam is deposited into a small region at the center of the crystal. Therefore, only a small central portion of the crystal was modeled where there was an appreciable thermal gradient. The coolant flowed in the direction of the incident beam. Due to the relatively high thermal conductivity of silicon and the large heat transfer coefficient of gallium, there is very little spreading of the heat in the plane of the crystal. Therefore, only a few channels absorb the incident power. Referring to Fig. 2, it is seen that the crystal contains two mirror planes of symmetry. If the total power absorbed by the fluid is not too great so that it does not heat up appreciably, then only one fourth of the crystal need be modeled. However if the gallium heats up enough, the symmetry is reduced to a single mirror plane and half of the crystal should be modeled, and the change in temperature of the coolant as it flows through the channels should be included. The crystal was modeled using linear 3-D isoparametric thermal elements (STIF 70). For the half-plate model the liquid gallium was modeled using transient thermal-flow elements (STIF 66).

From the experimental data, it was noticed that for a flow rate of 1 gpm the rocking curve became noticeably asymmetric above about 30 mA. This is apparently due to the heating of the gallium as it passes through the crystal. Two finite element models were analyzed. The first is a quarter-plate model with a constant fluid temperature. The second is a half-plate model that accounts for the temperature change in the fluid. A contour plot of the crystal surface temperatures for a beam current of 60 mA is shown in Fig. 3. The temperature increases in the downstream direction due to absorption of heat by the fluid. Also, the temperature gradient rapidly decreases down the length of the fin. Most of the heat is convected to the gallium near the top of the channel, and consequently, deep channels are not beneficial from a heat transfer point of view.

The thermophysical properties of silicon and gallium were allowed to vary as a function of temperature. The inlet gallium temperature was 50° C. The properties for gallium and silicon over the temperature range of 50-250 °C are given in Table 2. It should be noted that Young's modulus and Poisson's ratio vary for different directions in the crystal. Young's modulus is a maximum along the (111) direction for silicon and germanium.

Table 2. Thermal and physical properties of gallium and silicon in 50-250 °C range.

Material property	Gallium	Silicon
Thermal conductivity (W/m/K)	25 - 50	168 - 73
Density (kg/m^3)	6080	2330
Specific heat (J/kg/K)	343	686 - 850
Thermal coefficient of expansion (°C)$^{-1}$	NA	2.48 - 3.58e-6
Dynamic viscosity (N s/m^2)	1.7e-3	NA
Young's modulus along (111) (x10^{11} Pa)	NA	1.875
Young's modulus along (110), (112) (x10^{11} Pa)	NA	1.69
Poisson's ratio, $\nu_{(111),(1\bar{1}0)}$	NA	0.181
Poisson's ratio, $\nu_{(1\bar{1}0),(11\bar{2})}$	NA	0.262
Poisson's ratio, $\nu_{(11\bar{2}),(111)}$	NA	0.163

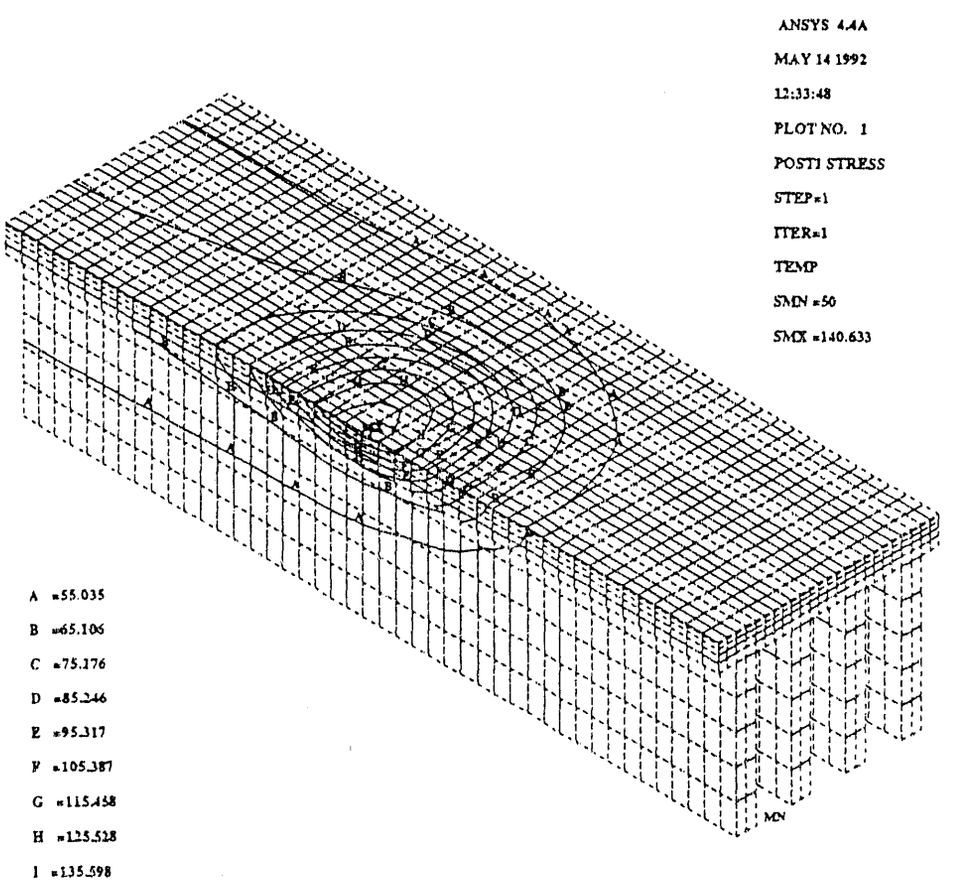

Fig. 3. Surface temperature on cooled first crystal for an electron beam current of 60 mA.

4.2.1 Heat transfer coefficient

Liquid metals are characterized by extremely large heat transfer coefficients. Under laminar flow conditions, heat transfer is controlled by molecular conduction and the correlations developed for ordinary fluids may be applied to liquid metal heat transfer. Values for the laminar Nusselt number for rectangular slots for various boundary conditions are given by Shah and London[8]. For turbulent convection, heat transfer is a function of both molecular and eddy conductivity. For normal fluids, such as water, the eddy conductivity is the dominant mode of heat transfer for turbulent flows. Molecular conduction is appreciable only near the solid interface. For liquid metals, molecular conduction is of the same order of magnitude as the eddy conduction even into the turbulent core. Therefore, the normal heat transfer correlations are not applicable to turbulent forced convection of liquid metals.

A great deal of experimental work has been done on liquid metal heat transfer. Correlations for the average Nusselt number in turbulent flow are usually given in the following functional form

$$Nu = c_1 + c_2 Pe^n \tag{8}$$

where c_1 and c_2 are constants that in general depend on the thermal boundary conditions, Pe is the Peclet number, and n is a function of the flow boundary conditions. For turbulent channel flow, a number of correlation's have been developed for various boundary conditions and are reported in the open literature.[9-12]

From the reported correlations, the constant c_1 varies from 3.3 to 12.0 depending on the thermal boundary conditions and channel geometry. For the analysis presented here, the correlation due to Lyon,[11] $c_1 = 7.0$, $c_2 = 0.025$, and $n = 0.8$, was chosen. The average heat transfer coefficient is calculated from the following equation,

$$h(T) = \frac{k_f(T)}{D_h} Nu(T) \tag{9}$$

where D_h is the channel hydraulic diameter, and k_f is the fluid thermal conductivity. For a volume flow rate of 1 gpm, the Reynolds number based on the channel hydraulic diameter was 2650. This value would normally indicate a transition flow between laminar and turbulent, but, due to the abruptly changing flow path, it is believed that the flow should be treated as turbulent. The average heat transfer coefficient is a function of temperature and varies from 119,255 to 229,503 W/m^2/K over the temperature range of 50-250°C.

5. STRUCTURAL ANALYSIS

The calculated temperature field from the thermal finite element analysis is used to calculate the thermal stress field and deformation in the crystal. The bottom of the channel ribs are bonded to a thick silicon plate and are assumed to be fixed in space. The quarter-plate model possesses two planes of symmetry, and the half-plate model has one symmetry plane. For the structural analysis, the crystal was modeled using linear 3-D isoparametric solid elements (STIF 45).

Single crystal silicon is highly anisotropic. The elastic moduli depend on the direction in the crystal. The Young's and shear moduli and Poisson's ratios have been measured for silicon and germanium by Wortman and Evans.[13] Silicon possesses three orthogonal symmetry planes coinciding with the crystallographic axes. For a rigid coordinate system rotation, the stiffness and compliance coefficients are calculated from a tensor transformation.

The crystal used in these experiments was oriented with the (111) vector along the surface normal. The two orthogonal directions are the $(11\bar{2})$ perpendicular to the channels and the $(1\bar{1}0)$ along the channels. The Young's moduli and Poisson's ratios associated with these directions are given in Table 2.

6. DIFFRACTION SIMULATION

The final step in the analysis is to calculate the impact that the thermal distortion has on diffraction. A computer program was developed to calculate the rocking curve for a double crystal monochromator (DCM). The distortion profile from the finite element structural analysis is input to the program, and a rocking curve is calculated. The details of the program are discussed by Khounsary, et al.[14]

A rocking curve is obtained by convoluting the reflectivity curve of the first crystal with the second. Experimentally, it is measured by recording the diffracted intensity as the second crystal is rotated, or "rocked," through the Bragg angle. The Darwin width represents the angular acceptance of a perfect crystal over which diffraction will occur for a given wavelength. If both crystals of a DCM are perfect, then the diffracted beam will be at the maximum theoretical intensity. However, if the first crystal is thermally distorted, its reflectivity curve is broadened. Now, when the reflectivity of the first crystal is convoluted with the second, the rocking curve is broader, and the peak diffracted intensity from the DCM is decreased

7. COMPARISON OF CALCULATIONS WITH EXPERIMENT

The theoretical (unstrained), measured and calculated rocking curves for storage ring currents of 30 and 60 mA are shown in Figs. 4 and 5.

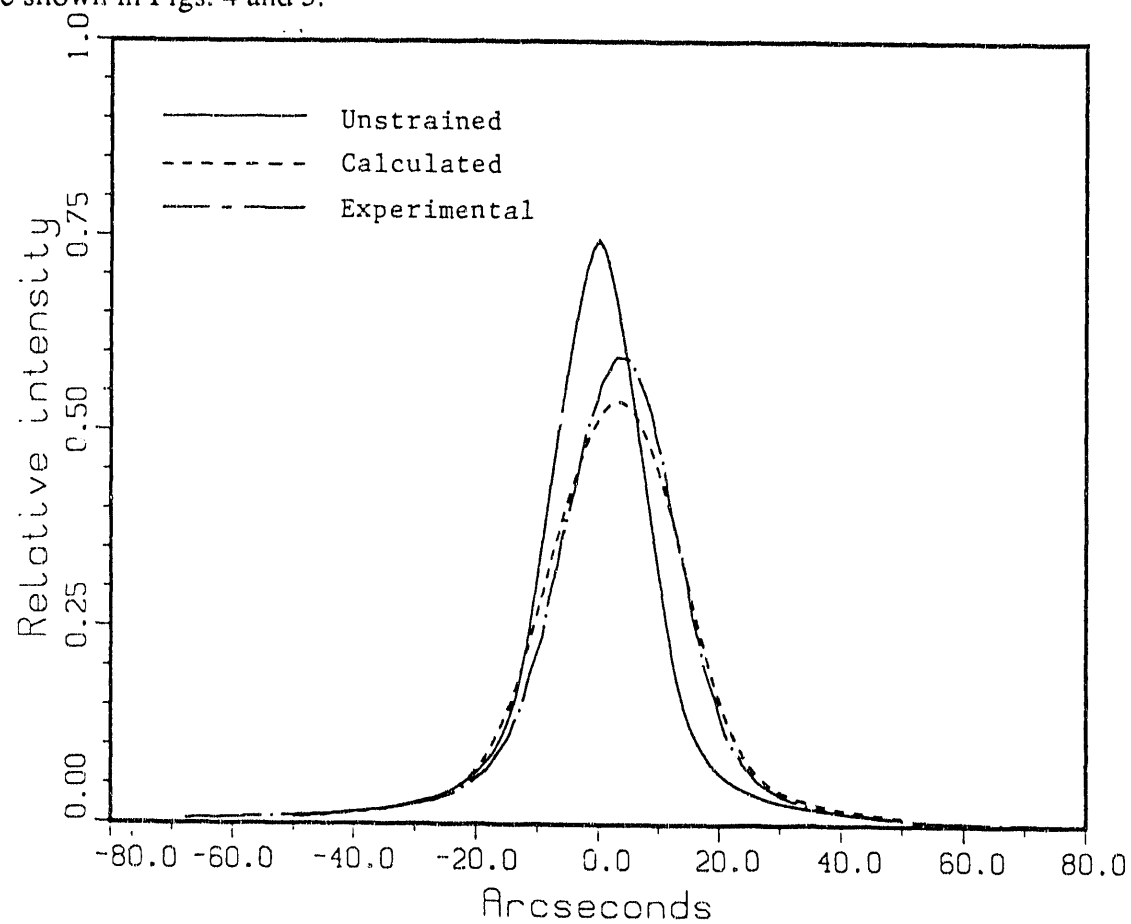

Fig. 4. Measured, calculated, and perfect theoretical rocking curves for 5 keV Si (111) at 30 mA.

For comparison, the areas under the measured and calculated rocking curves are set equal to the area under the unstrained curve. The peaks of the calculated and experimental curves are shifted due to the heating of the fluid, which shifts the distortion peak downstream.

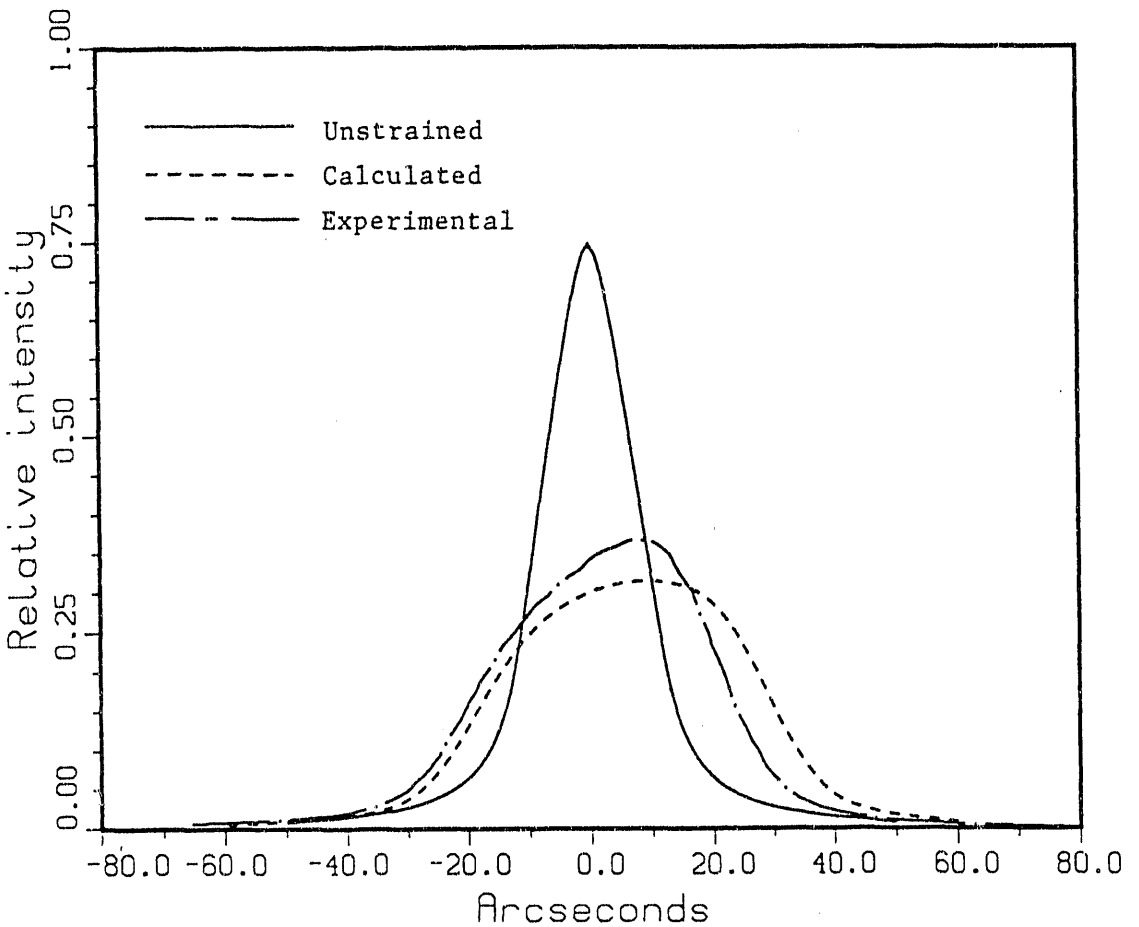

Fig. 5. Measured, calculated, and perfect theoretical rocking curves for 5 keV Si (111) at 60 mA.

The width of the measured and calculated rocking curves at full-width half-maximum (FWHM) as a function of storage ring current is shown in Fig. 6. Quadratic curve fits are drawn through the data points. It is shown that the half-plate model is somewhat better than the quarter-plate model. The finite element mesh densities were approximately equal for the two models. The discrepancy between the two is due to the fact that the half-plate model more realistically approximates the experimental situation. Because the fluid temperature rises as it passes through the channels, the temperature gradient in the crystal in the downstream direction is smaller than what is predicted by the quarter-plate model. Therefore, the half-plate model yields a more accurate result for the slope error. This conclusion is verified by the fact that the two calculated curves are diverging at higher currents. As the current increases, the rise in temperature of the fluid becomes more significant. The percent error from experiment in the half-plate model varies from about 5 percent at 10 mA to 15 percent at 60 mA. The most probable reason for the increasing error is that the mesh density is too coarse for the higher currents. As the current is increased the thermal gradients in the crystal increase, and, to maintain accuracy, the mesh density should also increase.

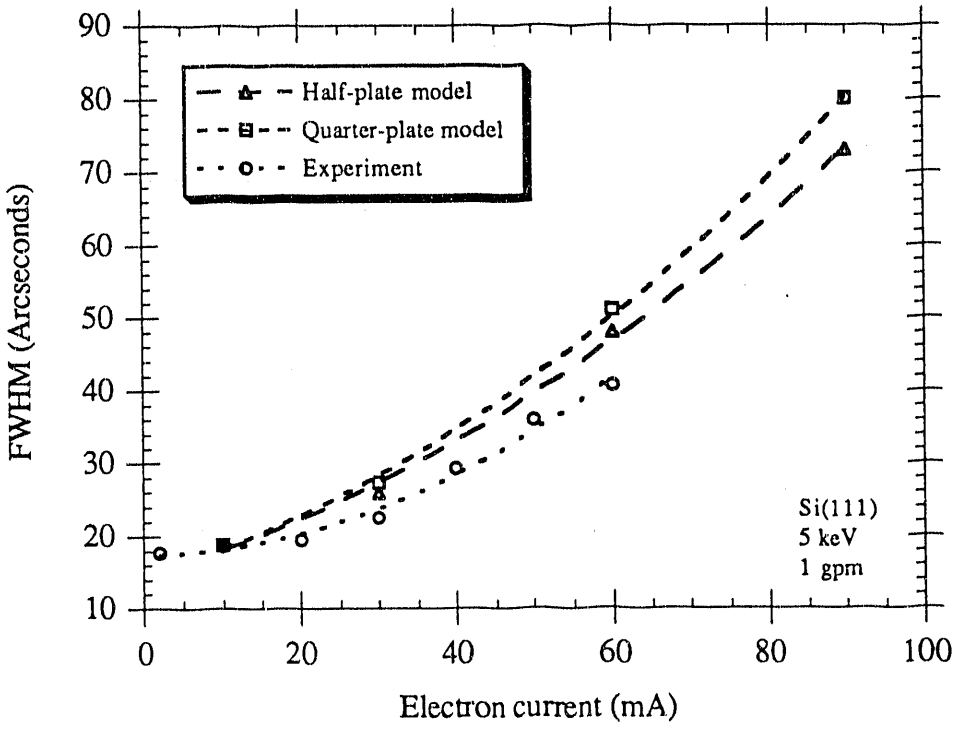

Fig. 6. Rocking curve full width at half maximum (FWHM) as a function of storage ring current.

8. CONCLUSIONS

It has been shown that the finite element method can be used to reliably predict the performance of high-heat-load x-ray optics. The method outlined in this paper provides an accurate and quick procedure for determining the thermal deformation in single crystal monochromators. When the experimental situation is such that the cooling fluid temperature rises significantly, the half-plate model provides a more accurate result. However, since setting up the half-plate model is considerably more involved, the quarter-plate model can be used to provide a very quick approximation. In all models, it is important to determine the appropriate mesh density to provide accurate results over all experimental situations. The inclusion of the anisotropic material properties of single crystal silicon has a significant affect on the accuracy of the results, therefore, it should not be treated as isotropic. This method can be used to predict the affect of changing various experimental parameters without having to perform costly experiments, which allows the optical design engineer to perform "what if" simulations on the x-ray optics to develop the best cooling and structural parameters.

9. ACKNOWLEDGMENTS

This work was supported by the US Department of Energy, BES-Materials Science under contract no. W-31-109-ENG-38.

10. REFERENCES

1. G. K. Shenoy, P. J. Viccaro, and D. M. Mills, "Characteristics of the 7-GeV Advanced Photon Source: a guide for users," Argonne National Laboratory Report ANL-88-9, Feb. 1988.

2. A. T. Macrander, W. K. Lee, R. K. Smither, D. M. Mills, C. S. Rogers, and A. M. Khounsary, "High heat load performance of an inclined-crystal monochromator with liquid gallium cooling on the CHESS-ANL undulator," To be published in Nuclear Instr. and Methods in Phy. Research A.

3. ANSYS - A general purpose finite element program, Rev. 4.4A, Swanson Analysis Systems Inc., Houston, PA, USA.

4. D. H. Bilderback, G. W. Batterman, M. J. Bedzyk, K. Finkelstein, C. Henderson, A. Merlini, W. Schildkamp, Q. Shen, and J. White, "Performance of a hard x-ray undulator at CHESS," Rev. Sci. Instrum., vol. 60 (7), pp. 1419-1425, 1989.

5. Kwang-Je Kim, "Angular distribution of undulator power for an arbitrary deflection parameter K," Nuclear Instr. and Methods in Phy. Research, A246, pp. 67-70, 1986.

6. R. K. Smither, G. A. Forster, C. A. Kot, and T. M. Kuzay, "Liquid gallium metal cooling for optical elements with high heat loads," Nuclear Instr. and Methods in Phy. Research A, vol. 266, pp. 517-524, 1988.

7. D. Chapman, N. Bmur, N. Lazarz, and W. Thomlinson, "Photon: A program for synchrotron radiation dose calculations," Nuclear Instrum. and Methods in Phy. Research A, vol. 266, pp. 191-194, 1988.

8. R. K. Shah and A. L. London, *Advances in Heat Transfer, Supplement 1: Laminar Flow Forced Convection in Ducts*, Academic Press, New York, 1971.

9. V. I. Subbotin, A. K. Papovyants, P. L. Kirillov, and N. N. Ivanovskii, "A study of heat transfer to molten sodium in tubes," At. Energiya (USSR), vol. 13, pp. 380-382, 1962.

10. Reed, C. B. Convective heat transfer in liquid metals. In: Kakacec, S.; Shaw, R.; Aung, W., eds., *Handbook of Single Phase Convective Heat Transfer*. New York, NY: Wiley Press; 1987: Chap. 8.

11. R. N. Lyon, "Forced convection heat transfer theory and experiments with liquid metals, USAEC report ORNL-361, Oak Ridge National Laboratory, 1949.

12. J. P. Hartnett and T. F. Irvine, "Nusselt values for estimating turbulent liquid metal heat transfer in non-circular ducts, AIChE J., vol. 3, pp. 313-317, 1957.

13. J. J. Wortman and R. A. Evans, "Young's modulus, shear modulus, and Poissons's ratio in silicon and germanium," Journal of Applied Physics, vol. 36, 1965.

14. A. M. Khounsary, J. J. Chrzas, D. M. Mills, and P. J. Viccaro, "Performance analysis of high-power synchrotron x-ray monochromators," Optical Engineering, vol. 29, pp. 1273-1280, 1990.

END

DATE FILMED

8/24/92